Tribology International 163 (2021) 107158

Contents lists available at ScienceDirect

Tribology International

journal homepage: www.elsevier.com/locate/triboint

Analysis of transient mixed elastohydrodynamic lubrication in planetary roller screw mechanism

Guangwu Zhou, Yuhao Zhang, Zhongzheng Wang, Wei Pu *

School of Aeronautics and Astronautics, Sichuan University, Chengdu 610065, China

ARTICLE INFO

Keywords:
Planetary roller screw mixed EHL entrainment velocity Uneven friction distribution Transient behaviors

ABSTRACT

Previous lubrication studies for planetary roller screw (PRSM) are mainly concentrated on steady-state condition without the consideration of entrainment angle. However, PRSM always operates in transient situations with frequent startup and shutdown process. In this paper, uneven friction distribution, the influence of helix angle on lubricating properties and transient behavior in the roller-screw interface are analyzed comprehensively based on transient mixed-EHL model, which considers real three-dimensional (3D) machined roughness and arbitrary entrainment velocity. The results show that smaller helix angle is beneficial to improve the lubrication performance. Increasing the rotating speed and declining axial load can moderate the uneven friction distribution. Besides, a relatively large angular acceleration may enlarge the film thickness and reduce the friction at the shut down status. The numerical simulation model can be utilized as a design optimization tool for the PRSM.

杭州新创技术转载

1. Introduction

Planetary roller screw mechanism is the key component of electromechanical servo system in aeronautics and space applications, which converts rotational motion into linear motion (see Fig. 1). A comparison between the ball screw mechanism and PRSM shows that PRSM has longer service life and higher transmission accuracy though they are similar in transmission principle. In recent years, it has been widely used in machine tools, industrial robots, aerospace and other fields because of its compact structure and enormous carrying capacity.

However, due to heavy load, fast speed and frequent back-and-forth motion, PRSM is accompanied by serious friction heat generation and wear problems. The transmission efficiency, accuracy, and service life are affected by the lubrication state on the contact interface in PRSM significantly. Therefore, a comprehensive lubrication analysis from the mixed-EHL model is essential to PRSM structural design, life improvement, and efficiency loss minimization.

The kinematics, stiffness characteristics and friction heat of PRSM have been studied extensively but researches are rather scanty on the lubrication of contact interface in PRSM. Auregan et al [1]. simulated the wear behavior at the screw-roller contact interface by disk-ring experiment, and studied the wear problem under different lubrication conditions by changing the normal load, speed and slide-roll ratio. Ma et al [2]. studied the contact characteristics of PRSM considering sliding friction, which are verified by finite element method. Jones [3–5] and velinsky [6] established a relatively mature analysis method for the contact characteristics and kinematics of PRSM. Fu and Liu [7,8] then used different methods to solve the kinematics equations of PRSM, and compared with the experimental results. In addition, there have been many articles that focused on the contact load between threads and static stiffness in PRSM [9–12]. After that, Xie et al [13]. analyzed the elastohydrodynamic lubrication of screw-roller interface with roughness surface. Qiao et al [14]. established a heat estimation model of PRSM based on the heat grid method, and studied the friction heat generation under different working conditions through experiments. Li [15] et al. established a friction torque model of PRSM in roller damping, and used the finite element method to analyze the contact stress. Sandu [16] et al. proposed a theoretical model to calculate the power dissipation of PRSM considering the contact geometry and dynamics comprehensively, and verified it with the experimental method.

The numerical algorithms and computational efficiency of EHL has been studied by many scholars, which is carried on many machine parts. Venner [17] and Kweh [18] established a mixed EHL with two-dimensional real surface roughness. Zhu [19] and Ai [20] proposed a point EHL model based on digital 3D real surface roughness. At the same time, Zhu [21] and Hu [22] proposed a unified mixed EHL to simulate the transition of interface morphology from dry friction to full film lubrication. After that, many scholars made many progresses based on the ref [21,22], such as Wang et al [23]., Liu et al [24]., He et al [25].,

* Corresponding author.
E-mail address: pwei@scu.edu.cn (W. Pu).

https://doi.org/10.1016/j.triboint.2021.107158
Received 18 April 2021; Received in revised form 17 June 2021; Accepted 28 June 2021
Available online 2 July 2021
0301-679X/© 2021 Elsevier Ltd. All rights reserved.

Nomenclature

a_0, b_0	short and long semi-axis length of Hertz contact ellipse
A_s, A_n	equivalent cross-sectional area of screw and nut, respectively
C_s	contact stiffness of screw-roller interface
C_n	contact stiffness of nut-roller interface
d_s, d_n	nominal diameters of screw and nut, respectively
d_{n0}	external diameter of nut
E	effective Young moduli
f_{sri}	friction of i-th thread
F	applied load at contact interface
Fa	axial force of any roller
F_c	friction at contact area
F_{lc}, F_{cc}	friction at fluid lubrication and boundary lubrication area, respectively
$Fout$	axial force in PRSM
G	pitch error
G_L	limiting elatic shear modulus
G_N, G_R	spur and ring gear pitch circle radii, respectively
h	film thickness
h_0	normal approach of the two rigid body surfaces
$K_s(e)$	first kind of complete elliptic integral of screw side
$K_n(e)$	first kind of complete elliptic integral of nut side
L_S, L_R	lead of screw and roller, respectively
M_{fd}	dynamic friction offset moment
n	number of rollers
n_t	number of contacts at each side
p	pressure
p_l	fluid pressure
P	pitch
Q_{si}, Q_{ni}	normal load on screw side and nut side, respectively
r_S, r_R	contact radii of the screw and roller, respectively
r_{S0}, r_{R0}	nominal radii of the screw and roller, respectively
R_1, R_2	equivalent radii of curvature for roller and screw, respectively
R_x, R_y	equivalent radii of curvature in the x-axis and y-axis directions, respectively
t	time
U_1, U_2	velocity for roller and screw, respectively
V	surface deformation
x, y	coordinates (x is chosen to be parallel to rolling direction)
x_{in}, x_{out}	x-coordinates at boundary
y_{in}, y_{out}	y-coordinates at boundary
z	number of starts
α_s	helix angle of screw
$\tilde{\alpha}$	pressure-viscosity exponent
β	contact angle
$\dot{\gamma}$	shear rate
δ_1, δ_2	roughness heights for surfaces 1 and 2
ε_i	pitch deviation
ε_p	pressure convergence accuracy
$\zeta_{R/S}$	angular velocity ratio
η	lubricant viscosity
η_0	ambient lubricant viscosity
θ_{CS}, θ_{CR}	angle of location of contact point
θ_e, θ_s	entraining and sliding vector angle
μ	friction coefficient
μ_e, μ_s	entraining and sliding velocity
ν	poisson's ratio
v_{s-r}	slip velocity of screw-roller interface
σ_R	composite root mean square roughness
τ	shear stress
τ_L	limiting shear stress
ρ	lubricant density
ρ_0	ambient lubricant density
$\sum\rho_s$	curvature sum of screw-roller interface
$\sum\rho_n$	curvature sum of nut-roller interfaces
ω_R	angular velocity of roller revolution
ω_s	angular velocity of screw
Ω	numerical solution domain

杭州新剑技术授权

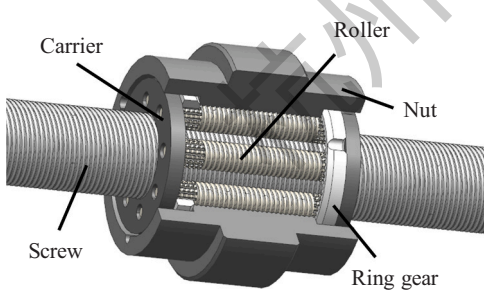

Fig. 1. Planetary roller screw mechanism.

Lubrecht et al [26]., and so on. Many scholars make some progress in the algorithm to solving the ultra-thin lubricant film, including the Newton-Raphson iterative [27], converse solution [28], multigrid algorithm [29–31] and simplified multigrid technique [32]. Later, Pu et al [33]. proposed a Mixed-EHL model for discretionary entrainment angle. It is worth mentioning that the previous EHL model can only calculate the condition when the entrainment angle is zero. In the transient EHL model of spiral bevel gears established by Wang [34], the equivalent curvature radius, entrainment velocity and contact load all change with time. As EHL is relatively mature, this paper will not elaborate on it. For details, please refer to Zhu [35,36].

Previous lubrication studies in PRSM were limited mostly to the steady-state cases with smooth surfaces, which ignored the effect of entrainment angle. The considerable start up and shut down process of PRSM represent that transient behavior can not be neglected in the analysis of EHL. In the present study, a comprehensive analysis for uneven friction distribution, the influence of helix angle on lubrication characteristic and transient behavior in the roller-screw interface is carried out by recently developed transient mixed-EHL model [34], which considers 3D roughness surface and discretionary entrainment velocity. The results of new developed mixed-EHL Model for roller-screw interface show that the simulation method can be used as a design optimization tool for the PRSM and is beneficial to the study of wear, temperature and fatigue life.

2. Theoretical method

2.1. Load distribution

The main force transmission parts of PRSM include screw, nut and several rollers. The threads of screw and nut are usually designed as trapezoidal thread with 90-degree angle to obtain excellent transmission efficiency. The profile of roller threads is designed as an arc for the sake of reducing the friction between parts. Therefore, the contact types of nut-roller and screw-roller can be regarded as point contact. Due to the bearing behavior of the thread contact mechanism, the load distribution between threads will be uneven. The normal contact forces at the screw-roller and nut-roller side are expressed as Q_{si} and Q_{ni} respectively, where

the subscript $i = 1 \sim n_t$ and n_t is the number of roller threads.

According to the load balance condition, the axial force of screw is explicated as:[12].

$$Fa = \frac{Fout}{n} = \sum_{i=1}^{n_t} Q_{si}\sin\alpha_s\cos\beta = \sum_{i=1}^{n_t} Q_{ni}\sin\alpha_s\cos\beta \tag{1}$$

where β is the contact angle, α_s is the helix angle, and n is the number of rollers.

The contact stiffness (C_s and C_n) of the screw-roller and nut-roller depend on the structural and material parameters, which can be expressed as:

$$\left\{\begin{array}{l} C_s = \dfrac{K_s(e)}{\pi ma_s}\sqrt[3]{(3E)^2\sum\rho_s/4} \\ C_n = \dfrac{K_n(e)}{\pi ma_n}\sqrt[3]{(3E)^2\sum\rho_n/4} \end{array}\right\} \tag{2}$$

where $K_s(e)$ and $K_n(e)$ are the first kind of complete elliptic integral; E represents the effective Young moduli; ma_s and ma_n are the coefficient related to eccentricity of the screw side and nut side respectively; $\sum\rho_s$ and $\sum\rho_n$ are the curvature sum of roller-screw and roller-nut contacts, respectively.

Under the deformation compatibility condition of threads, the contact load distribution is expressed as:[37].

$$Qs_{(i-1)}^{(2/3)} = Qs_i^{(2/3)} + \frac{(\varepsilon_{(i-1)} - \varepsilon_i)\sin\alpha_s\cos\beta}{C_s + C_n} + \frac{nP(A_s + A_n)\sum_{j=i}^{\tau} Qs_i\sin^2\alpha_s\cos^2\beta}{4EA_sA_n(C_s + C_n)} \tag{3}$$

Where P is the pitch; ε_i is the pitch deviation; $A_s = \pi d_S^2/4$ and $A_n = \pi\left(d_{n0}^2 - d_n^2\right)/4$ are the equivalent cross-sectional areas; d_S and d_n are the nominal diameters; and d_{n0} is the external diameter of the nut. And all subscripts s and n denote screw and nut respectively.

2.2. Contact kinematics

When the roller rotates around the axis of the screw, it also rotates around its own axis. The results of ref [2] show that the relative sliding speed at nut-roller interface is much lower compared with screw-roller interface. Moreover, the rolling speed of the contact points between nut and roller is close to zero without considering pitch circle mismatch of the spur-ring gear [3]. Therefore, the contact behavior of the roller-nut interface is regarded as pure rolling in this paper.

However, the rotational motion of the roller is purely due to the friction at the roller-screw interface. The friction of roller-screw interface is the most important factor on transmission performance. Generally, the thread directions of screw and roller are designed to be opposite to obtain large pitch and small lead. The research results of ref [5] show that the contact point of the screw and roller deviates from the center line of the PRSM. And the deflection angle (θ_{CS} and θ_{CR}) is used to determine the position of the contact point.

In order to determine the direction of the sliding speed of the screw-roller interface, the coordinate system $X_{scj}Y_{scj}Z_{scj}$ is established as shown in Fig. 2. The origin is always on the central axis of PRSM, and X_{scj} always points to the center of the j-th thread.

Using the method of ref [6], the relative slip velocity v_{s-r} of screw-roller interface can be calculated as

$$v_{s-r} = \left\{\begin{array}{c} (-r_s\sin\theta_{CS}\omega_s + r_R\sin\theta_{CR}G\omega_R)X_{scj} \\ (r_s\cos\theta_{CS}\omega_s - r_{R0}\omega_R - r_{S0}\omega_R - r_R\cos\theta_{CR}G\omega_R)Y_{scj} \\ \left(\dfrac{L_S}{2\pi}\omega_s - \dfrac{L_S - L_R}{2\pi}\omega_R - \dfrac{GL_R}{2\pi}\omega_R\right)Z_{scj} \end{array}\right\} \tag{4}$$

Among them, L_S and L_R are the lead of screw and roller respectively; r_s and r_R are the actual contact radii of the screw and roller; r_{R0} and r_{S0} are the nominal radii of the roller and scre-w.

The spur ring gear is designed at both ends of the rollers to prevent the axial slip between the roller-nut interface. The pitch error between the spur ring gear and screw thread has some influence on the slip at the screw-roller interface as well.

$$G = (G_N - G_R)/G_R \tag{5}$$

Where G_N and G_R are the spur and ring gear pitch circle radii respectively.

In steady state, the ratio of common angular velocity of roller ω_R and angular velocity of screw ω_S only depends on the structural parameters of PRSM and is not related to the force state of screw. The expression is as follows:

$$\zeta_{R/S} = \frac{\omega_R}{\omega_s} = \frac{Gr_Sr_R\sin\theta_{CS}\sin\theta_{CR} + r_s\cos\theta_{CS}(r_{R0} + r_{S0} - Gr_R\cos\theta_{CR})}{(-Gr_R\sin\theta_{CR})^2 + (r_{R0} + r_{S0} - Gr_R\cos\theta_{CR})^2} \tag{6}$$

2.3. Mixed EHL equations

Zhu and Pu [33] proposed an elliptical contact EHL model with arbitrary entrainment angle, which is now applied to the analysis of lubrication behavior at the screw-roller interface in this paper.

Normal load and relative sliding velocity are solved by Eq.3 and Eq.5 respectively. The relationship between contact ellipse and principal direction of screw is shown in Fig. 3. The direction of relative sliding velocity solved by Eq.5 is close to PRS rotation axis. The angles (θ_e, θ_s) between velocity vectors (μ_e, μ_s) and x axis are illustrated in Fig. 3 (The velocity vectors μ_s is equal to the relative slip velocity of screw-roller interface v_{s-r}). The entrainment velocity μ_e, which can be seen as the rolling speed of roller and screw in the contact points, can be calculated as following:

$$\mu_e = \omega_s r_s\cos\alpha_s \tag{7}$$

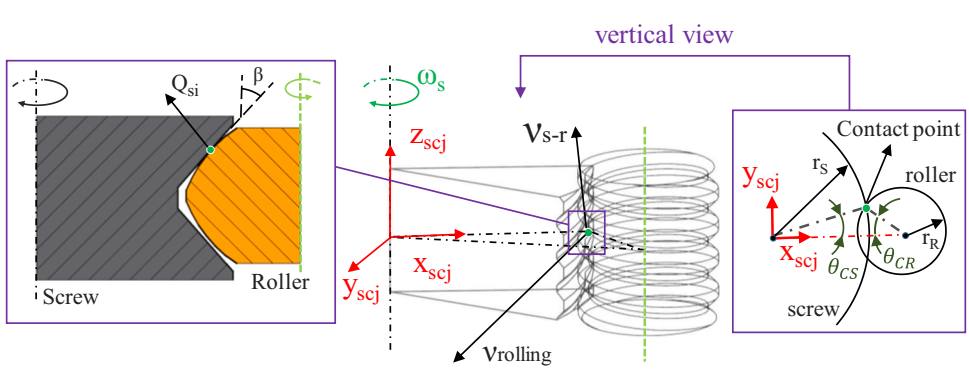

Fig. 2. The contact geometry of the roller and screw.

杭州新剑技术转载

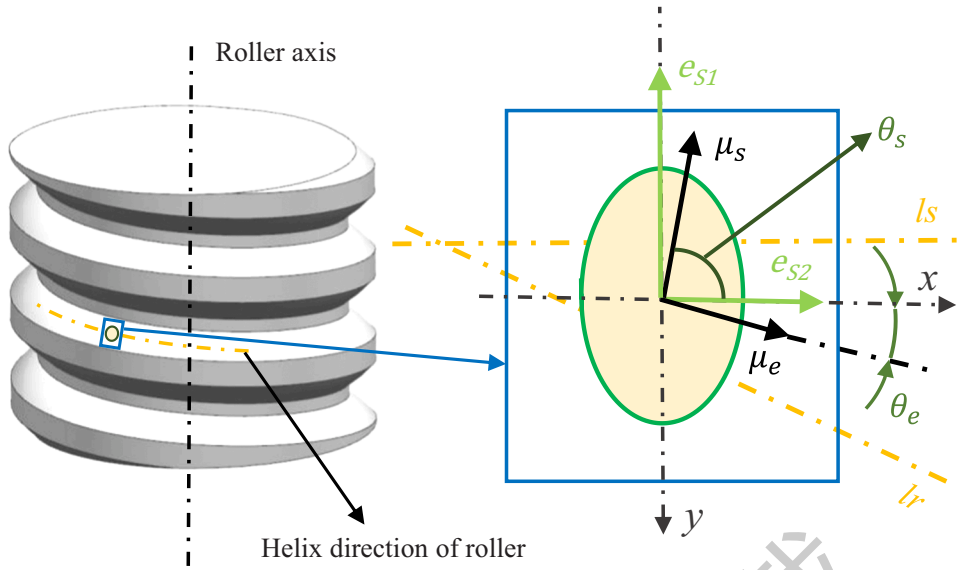

Fig. 3. The direction of sliding and entraining vector in the roller-screw interface.

It can be seen that *ls* and *lr* represent the helix direction of screw and roller respectively; e_{S1} and e_{S2} are the direction of maximum and minimum curvature radius of screw contact geometry respectively; x and y are coordinates of solution domain; and the blue border is the numerical simulation solution domain.

The contact pressure and film thickness are solved by Reynolds equation:[33].

$$\frac{\partial}{\partial x}\left(\frac{\rho h^3}{12\eta}\frac{\partial p}{\partial x}\right)+\frac{\partial}{\partial y}\left(\frac{\rho h^3}{12\eta}\frac{\partial p}{\partial y}\right)=\mu_e(t)\cos[\theta_e(t)]\frac{\partial(\rho h)}{\partial x}+\mu_e(t)\sin[\theta_e(t)]\frac{\partial(\rho h)}{\partial y}+\frac{\partial(\rho h)}{\partial t} \tag{8}$$

Due to the quite limited effects of heat actually, the isothermal EHL model is used in this paper [38]. Either the non-Newtonian or Newtonian lubricant can be assumed in the solution of Reynolds equation. In the example of non-Newtonian lubricant, η is replaced by the effective viscosity for the inlet conditions. More information can be found in Refs [19,22].

In addition, the boundary conditions of pressure in the solution region are as follows:

$$p_l(x_{in}, y\quad)=p_l(x_{out}, y\quad)=p_l(x, y_{in}\quad)=p_l(x, y_{out}\quad)=0 \tag{9}$$

Where, p_l is the fluid pressure, x_{in}, x_{out}, y_{in} and y_{out} are the coordinates at boundary of the solution area. As the solution area is much larger than the elliptical contact area, the contact at boundary is fluid contact and the fluid pressure at boundary is zero.

The film thickness is a function of the time t of the specified point, including the effect of contact geometry, elastic deformation and roughness. The expression is as follows :

$$h(x,y,t)=h_0(t)+\frac{x^2}{2R_x}+\frac{y^2}{2R_y}+V(x,y,t)+\delta_1(x,y,t)+\delta_2(x,y,t) \tag{10}$$

Where, $h_0(t)$ is the normal proximity of the two contact surfaces, $x^2/2R_x$ and $y^2/2\,R_y$ are the contact geometry before elastic deformation, $\delta_1(x,y,t)$ and $\delta_2(x,y,t)$ denote machined rough surfaces 1 and 2 respectively.

The expression of Boussinesq integral, used for solving the surface deformation $V(x, y, t)$, is as follows:

$$V(x,y,t)=\frac{2}{\pi E}\iint_{\Omega}\frac{p(\xi,\varsigma,t)}{\sqrt{(x-\xi)^2+(y-\varsigma)^2}}d\xi d\varsigma \tag{11}$$

The viscosity of lubricants depends on the pressure to a certain extent. The viscosity equation of exponential law is used for calculation in this paper:

$$\eta=\eta_0 e^{\tilde{\alpha}p} \tag{12}$$

Where, η_0 is the initial viscosity of lubricant, $\tilde{\alpha}$ is the pressure-viscosity exponent.

The relationship between pressure and density can be expressed as: [39].

$$\rho=\rho_0\left(1+\frac{0.6\times10^{-9}p}{1+1.7\times10^{-9}p}\right) \tag{13}$$

At any time, there is an equilibrium relationship between the applied load and the pressure in the whole solution domain as follows:

$$F(t)=\iint_{\Omega}p(x,y,t)dxdy \tag{14}$$

3. Numerical procedure

The dimensionless governing equations in 2.3 are solved numerically based on the Newton iteration method. In order to make the obtained pressure distribution satisfies certain convergence accuracy, the DC-FFT method is used [40]. The Gauss Seidel iterative method and semi system algorithm are developed for obtaining high convergence accuracy for mixed EHL with ultra-thin films. The contact pressure and film thickness are obtained by solving Reynolds equation. Furthermore, the PMD algorithm can improve the calculation efficiency and accuracy significantly. And the ability to solve the very thin film thickness will improve as grid density rises. The transient PMD method of three-layer grid [34] is used in the calculation process. The program converges from relatively sparse grid I to relatively dense grid II, and converges to the most precise grid III eventually. The convergence results of pressure and film distribution of the upper grid are taken as the initial values of the next grid. The calculation flow diagram of transient EHL is shown in Fig. 4.

In order to obtain good accuracy of numerical simulation, it is necessary to satisfy the Newton Raphson iterative convergence criterion of Reynolds equation. The expression is as follows:

杭州新剑授权转载

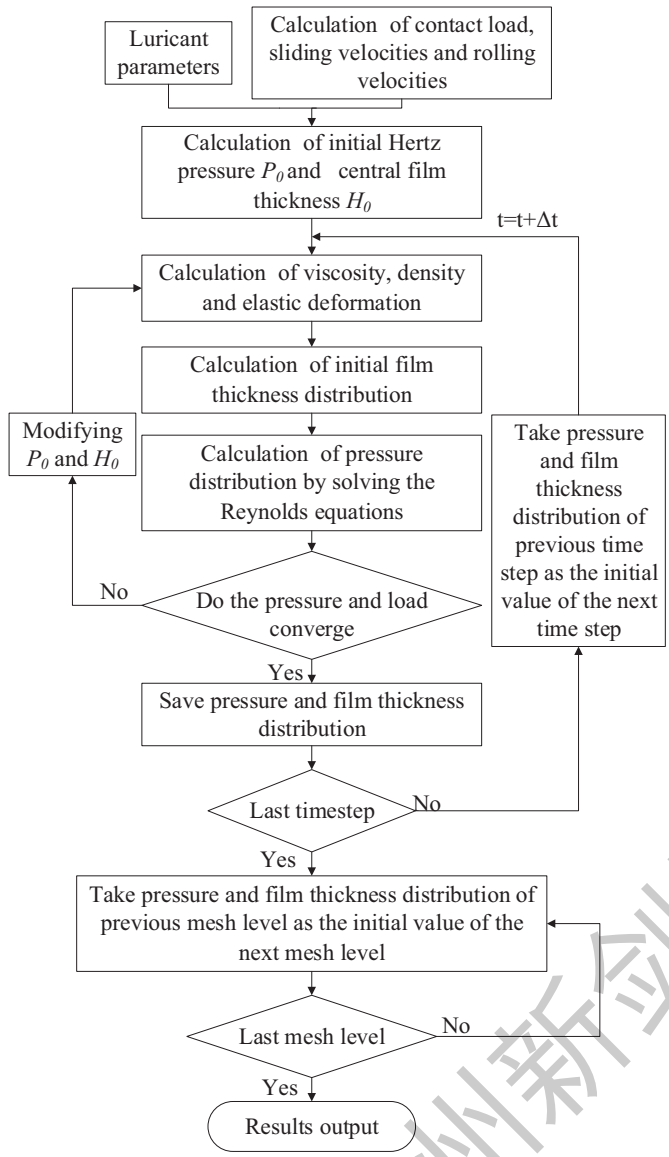

Fig. 4. Flowchart of transient EHL in PRSM.

$$\varepsilon_p = \frac{\sum\sum\left|p_{i,j}^{new} - p_{i,j}^{old}\right|}{\sum\sum p_{i,j}^{new}} \le 1 \times 10^{-6} \tag{15}$$

where, $p_{i,j}$ is the pressure distribution obtained through solving the Reynolds equation.

In addition, the friction at the contact area, obtained by the numerical simulation of Mixed-EHL, is caused by the boundary friction in dry contact area and lubricant shear stress. The expression is as follows:

$$\left\{\begin{array}{c} F_c = F_{lc} + F_{cc} \\ \mu = F_c/Q \end{array}\right\} \tag{16}$$

where, F_c is the friction at the contact area; μ is the friction coefficient; Q is the normal force at the contact interface; F_{lc} and F_{cc} are lubricant shear stress and the friction at the boundary lubrication area respectively.

Commonly, the constant value of boundary friction coefficient is between 0.07 and 0.15(film thickness is 0 or close to 0). For the fluid lubrication area, the oil film shear stress is calculated by the Bair-winer non-Newtonian rheological method. The expression is as follows:

$$\left\{\begin{array}{c} \dot{\gamma} = \dfrac{\dot{\tau}}{G_L} - \dfrac{\tau_L}{\eta}\ln\left(1 - \dfrac{\tau}{\tau_L}\right) \quad h > 0.5nm \\ \tau = 0.15p \quad h \le 0.5nm \end{array}\right\} \tag{17}$$

Where, the ultimate shear stress τ_L and ultimate shear elastic modulus G_L are obtained by experiments.

4. Results and discussion

4.1. Basic parameters

The design parameters of PRSM calculated by numerical simulation of this model are shown in Table 1(Material parameters see Table 2). The solution domain[$-2.0a_0 \le x \le 2.0a_0$, $-1.5a_0 \le y \le 1.5a_0$] and the grid density (256 ×256) are used. The roughness of the actual machined surface, measured with an optical profilometer, is employed in this paper (The numerical simulation cases with the actual machined surface will be marked with Rough). The surface roughness of screw and roller are set to be 0.4 μm indicated by Rq, and the corresponding root mean square (RMS) roughness is equal to 4 μm. The 3D morphology of rough surface is illustrated in Fig. 5.

4.2. Effect of helix angle on lubrication

The helix angle has a crucial influence on the bearing characteristics, transmission accuracy and efficiency. However, few people have studied the effect of helix angle on the lubrication performance of the screw-roller interface. In order to illustrate the effect of the helix angle on lubrication clearly, the helix angle of screw ($1deg \le \alpha_s \le 23.5deg$) that can change the entrainment velocity vector and the equivalent radii of curvature are selected for numerical simulation with and without considering the rough surface.

The differential geometry method is used to calculate the equivalent radius of curvature of the contact surfaces between the screw and the roller here [16]. R_1 and R_2 are the equivalent radii of curvature for roller and screw, respectively. Moreover, the velocity vectors of two contact surfaces in the directions of ellipse axes can be calculated as:

$$\left\{\begin{array}{c} U_{1x} = |\mu_e|\cos\theta_e + |\mu_s|\cos\theta_s \\ U_{1y} = |\mu_e|\sin\theta_e - |\mu_s|\sin\theta_s \\ U_{2x} = |\mu_e|\cos\theta_e \\ U_{2y} = |\mu_e|\sin\theta_e \end{array}\right\} \tag{18}$$

Among them, the subscripts 1 and 2 represent the contact surfaces of roller and screw respectively.

The variations of equivalent radii of curvature and entraining velocity with different helix angle are shown in Fig. 6. The helix angle would change, leading to the variations of several parameters, including equivalent radius of curvature in contact surface, the magnitude and direction of entrainment velocity.

The screw speed $\omega_s = 40rad/s$, the normal force Q = 43 N, the helix angle $\alpha_s = \{1.5, 7.5, 13.5, 19.5, 23.5\}deg$ is calculated in Fig. 7. The film distributions will form a "horseshoe" shape due to the joint action of the entrainment angle and the extrusion effect. It is illustrated in Fig. 7 that

Table1
Basic structure parameters of PRS.

Parameters	Values
Nominal radius of screw, r_{S0}	12 mm
Nominal radius of roller, r_{R0}	4 mm
Nominal radius of nut, r_{N0}	20 mm
Pitch, P	1.5 mm
Number of contacts at each side, n_t	30
Pressure angle, β	45 deg
Number of rollers, n	8
Number of starts, z	3

杭州新剑技术转载

Table2
material parameters of PRS.

Parameter	Value
Young's modulus of body 1/2, E	212 GPa
Poisson's ratio of body 1/2, ν	0.29
Lubricant viscosity, η_0	0.169(Pa·s)
pressure viscosity coefficient, $\tilde{\alpha}$	34.016 Pa^{-1}

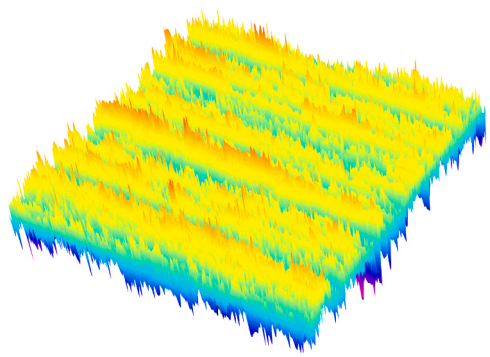

Fig. 5. 3D rough surface morphology.

the direction of "horseshoe" film distribution area changes with the increase of helix angle.

Generally, the magnitude of film thickness is close to roughness of contact area, even less than the roughness. Therefore, it is necessary to consider the influence of roughness in EHL simulation. Fig. 8 shows the lubrication properties of contact area with different helix angle, which considers real 3D machined roughness. From the cloud image of film thickness distribution, the bright yellow areas that indicate the asperity contacts or dry contact rise with the increment of helix angle. Besides, the peak pressure in the pressure contours increases with the increment of helix angle, which causes large plastic deformation and pitting on the contact surface.

Film thickness ratio λ, is the average film thickness divided by the composite RMS roughness of two contact surfaces. The expression is as follows:

$$\lambda = \frac{h_a}{\sigma_R} \tag{19}$$

Where, h_a is the average film thickness, σ_R is the composite RMS roughness. In fact, the lubricating properties in the contact interface is usually measured by film thickness ratio. Besides, the contact load ratio W_c is the ratio of the load carried by dry contacts over the total load in the contact area. More details can be found in Refs [41].

Other parameters remain unchanged. Fig. 9 shows that the film thickness ratio λ has a declining trend at first and then it rises very gently as the helix angle increases. Conversely, the friction coefficient μ and contact load ratio W_c increase at the beginning and then drop in small

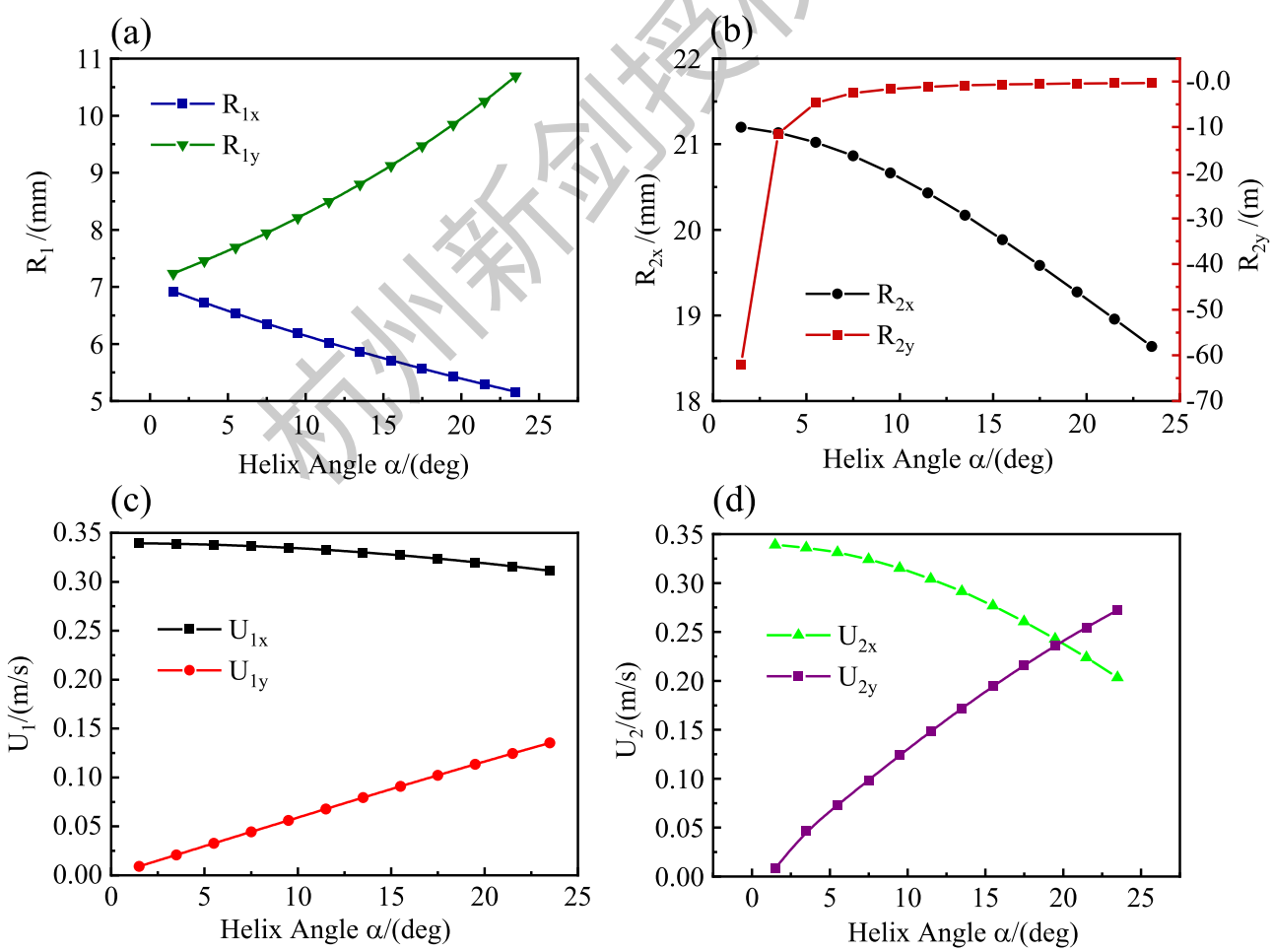

Fig. 6. Variations of equivalent radii of curvature and entraining velocity. (a) Equivalent curvature radius of roller (b) Equivalent curvature radius of screw (c) entraining velocity for roller and (d) entraining velocity for screw.

杭州新剑授权转载

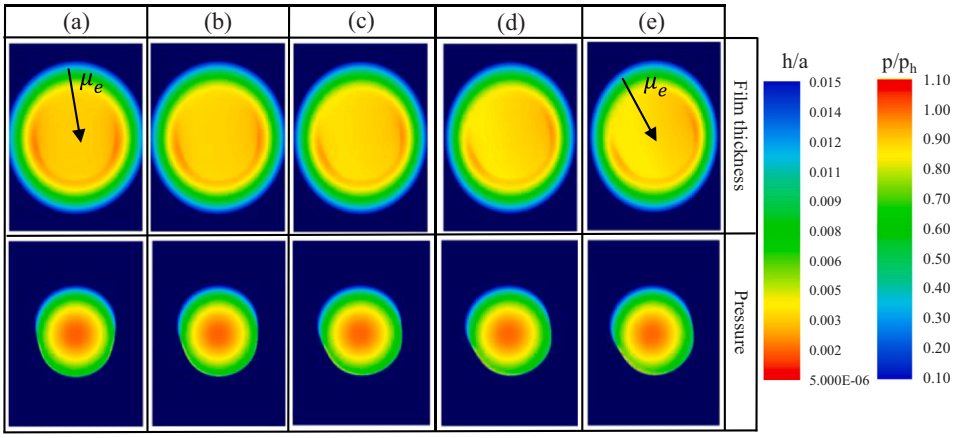

Fig. 7. Film thickness and pressure contours for different helix angle (Smooth, $\omega_s = 40rad/s$). (a) a_s= 1.5 deg (b) a_s= 7.5 deg (c) a_s= 13.5 deg (d) a_s= 19.5 deg and (e) a_s= 23.5 deg.

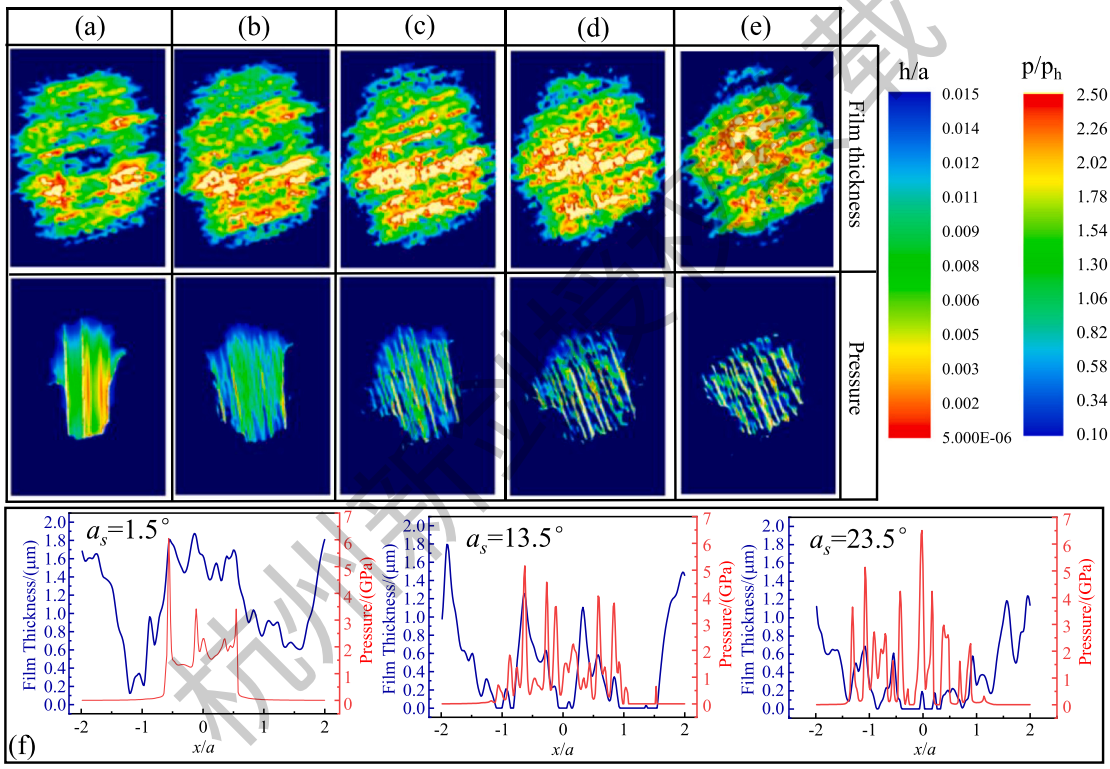

Fig. 8. Film thickness and pressure for different helix angle (Rough, $\omega_s = 40rad/s$). (a) a_s= 1.5 deg (b) a_s= 7.5 deg (c) a_s= 13.5 deg (d) a_s= 19.5 deg (e) a_s= 23.5 deg and (f) film thickness and pressure in the X rolling direction.

degree with the increment of the helix angle. The increment of contact load ratio will inevitably lead to the increment of boundary lubrication area. Therefore, the coefficient of friction will have the same variation trend compared with contact load ratio.

The results of the ref [6] show that when the helix angle is beyond 10 deg, the PRSM has outstanding transmission efficiency. But the small helix angle can make the contact interface have a good lubrication performance. Reasonable selection of the helix angle, the design parameters, can optimize the comprehensive performance of the PRSM.

4.3. The uneven distribution of friction between threads

The uneven load distribution between threads is a common phenomenon in all threaded components, and PRSM is inevitable. The uneven load distribution will lead to the difference of lubrication and friction heat generation at each contact point unavoidably.

It is assumed that the axial force between all rollers are uniform and the geometry of each thread is the same. Fig. 10 shows the uneven friction distribution with the axial load $Fa = 12$ kN, screw speed $\omega_s = 10rad/s$ and the pitch error (± 8 μm) that obey normal distribution N (0, 2.25), which is generated by random function. It is worth noting that the distribution of friction is consistent with that of load distribution considering pitch deviations. Generally, the larger the load, the more serious the wear of contact area. As ref [11] said, the load distribution with pith deviations and wearing volume of screw threads are in good agreement.

Moreover, the uneven friction distribution with different working condition are studied. The distribution of friction coefficient at all contact points is illustrated in Fig. 11. Friction coefficient decreases as the screw speed increases, and when the screw speed goes beyond

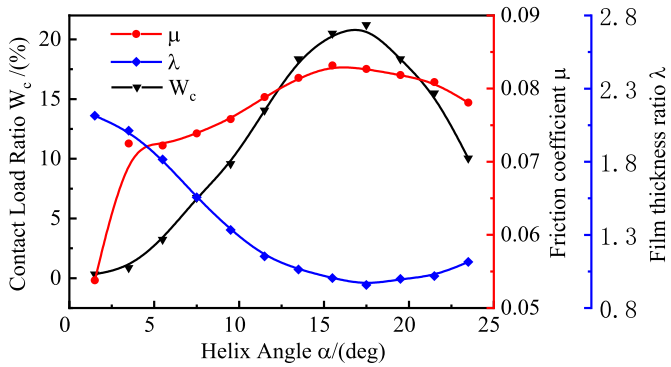

Fig. 9. Effect of helix angle on the film thickness ratio, contact load ratio and coefficient of friction.

60 rad/s, the friction coefficient gradually decreases.

The uneven friction distribution of threads may lead to the inclination of the roller motion to deviate from the own axis. However, the spur ring gear at both ends of the roller will limit this movement, thus aggravating the load bearing of the spur ring gear. The torque caused by the uneven friction distribution at all threads is defined as M_{fd} and its calculation expression is as follows:

$$M_{fd} = \sum_{i=1}^{n_t}\left(f_{sri}\frac{\boldsymbol{v}_{s-r}}{|\boldsymbol{v}_{s-r}|}\bullet\vec{\boldsymbol{c}}\right)\left(i-\frac{n_t}{2}\right)P \tag{20}$$

Where, $\vec{\boldsymbol{c}} = \{0,1,1\}$. The Z_{scj} component of the friction force acting on all threads is consistent with the direction of the roller axis, so it has no effect on the roller motion offset. In order to illustrate the offset tendency of roller caused by the uneven friction distribution intuitively, the direction and magnitude of friction and torque are exaggerated in Fig. 12. Actually, the larger dynamic friction offset moment may cause the inclination of roller motion and overload of spur ring gear.

Fig. 13 shows the dynamic friction offset moment of a single roller under different speeds and axial force. For a given screw speed, the roller with the lager axial force can possess a bigger offset moment than that with smaller axial force. And the offset moment also decreases with increasing rolling speed. As the axial load decreases, the change range of the offset moment declines as well. Besides, when the rotation speed is faster than 240 rad/s, the downward trend of M_{fd} becomes slower. Therefore, the increment of the screw speed is not only conducive to the lubrication of the screw-roller contact interface, but also beneficial to reduce the load of the spur ring gear. And the reduction of axial load is vital in improving the dynamics of roller and loading state of spur ring gear as well.

4.4. Transient behaviors in start up and shut down process

PRSM always operates in start-up and shut down process due to frequent linear feed conditions of back-and-forth motion. Therefore, it is necessary to discuss the pressure and film thickness distributions of screw-roller interface in the transient process.

The acceleration and deceleration rate of the screw are assumed to be constant during start up and shut down process. The variation of roller revolution speed ω_R, screw rotation speed ω_s and entraining velocity during two start up and shut down processes are shown in the Fig. 14.

The dynamic entraining velocity as input parameters is used in the numerical simulation of PRSM during start up and shut down process from the newly developed transient EHL model [31]. The normal load remains constant (Q=35 N). Fig. 15 shows the film thickness and pressure contours with smooth surface. The film thickness will thicken at first, followed by a downward trend during one start up and shut down period.

The film thickness-time curves (average film thickness h_a, central film thickness h_c and minimum film thickness h_m) during start up and shut down process are shown in Fig. 16. It can be seen that the variation trend in film thickness almost coincided with entraining velocity. The lubricant is trapped in the rough surface when entraining velocity is dropped to near zero, which is beneficial for the creation of lubrication film and separation of two contact surfaces. Therefore, the h_c of P_C (minimum value) in rough surfaces is higher than that in smooth surfaces during one start up and shut down process, as shown in Fig. 16.

Besides, P_A ($t = 5$ ms), P_B ($t = 10$ ms), P_C ($t = 11.2$ ms, minimum value of h_c) and P_D ($t = 15$ ms) are selected for four special points, as demonstrated in Fig. 17. It was observed that the film thickness curve of P_A coincided well with the curve of P_D. It is noted that film thickness drops as entraining velocity decreases to zero at P_A, but does not decrease to the minimum value. Film thickness would continue to fall to P_C with entraining velocity rises after 10 ms, which may be caused by the viscous effect of lubricants.

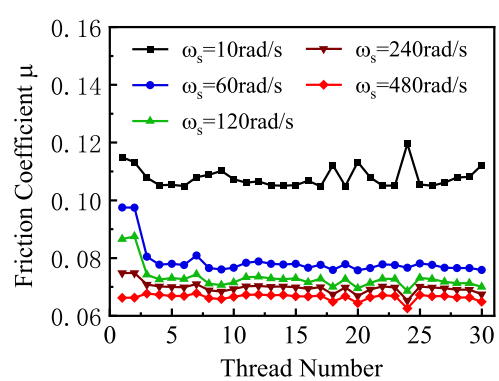

Fig. 11. Friction distribution in different screw speed.

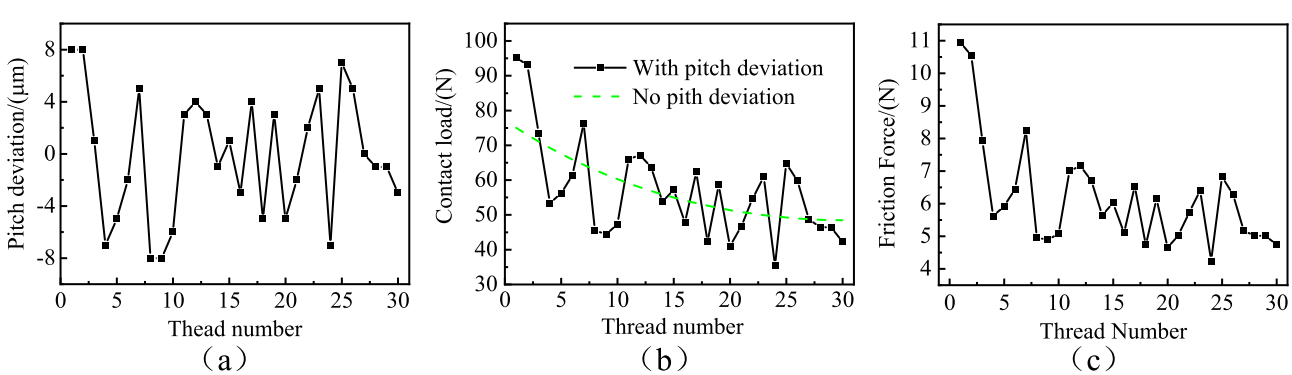

Fig. 10. Pith deviations (a), load distribution (b), friction distribution (c) of all threads.

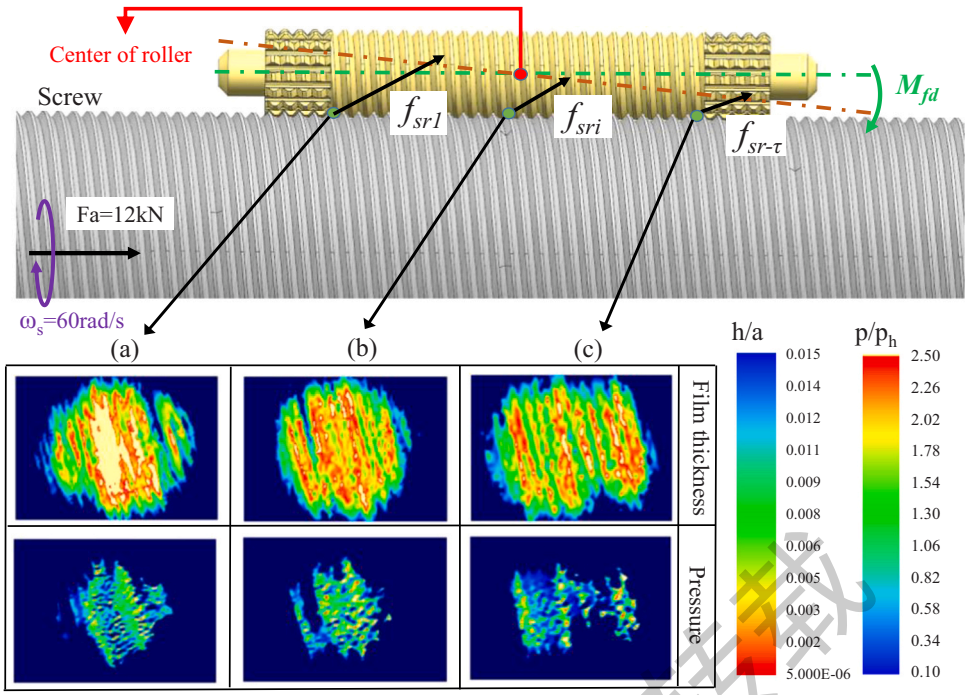

Fig. 12. The dynamic friction offset torque of single roller. (a) Lubrication performance of thread 1 (b) Lubrication performance of thread 12 and (c) Lubrication performance of thread 30.

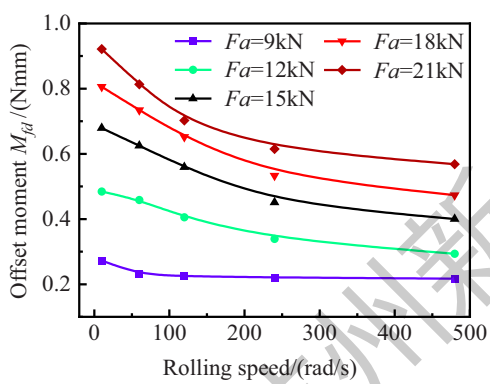

Fig. 13. Dynamic friction offset moment under different rolling speed and axial force.

The effect of 3D machined roughness is also analyzed. The film thickness and pressure contours using rough surface are plotted in Fig. 18. The lubrication regime seems to be enlarged during the start up process, and appears to be shrunken in time of shut down process.

In addition, the start up and shut down process with different angular acceleration are calculated. Fig. 19 shows the variations in rolling speed of screw (a), average film thickness (b), contact load ratio (c) and friction coefficient (d) during two start up and shut down process. The purple circles indicate the shut down status of back-and-forth motion. The lubrication at the shut down status varies considerably among different angular acceleration. The average film thickness at shut down status is smaller for smaller angular acceleration. In contrast, the smaller the angular acceleration, the higher the contact load ratio and friction coefficient. Therefore, larger angular acceleration is beneficial to improve the lubrication performance at contact area during the start up and shut down process.

Actually, the process of start up and shut down are two typical operating conditions in engineering inevitably, which means the PRSM undergoes the transformation of low-speed and heavy-load working conditions frequently. The results of numerical simulation predict the transient lubrication behavior of PRSM, which are beneficial for the following study of failure and efficiency loss.

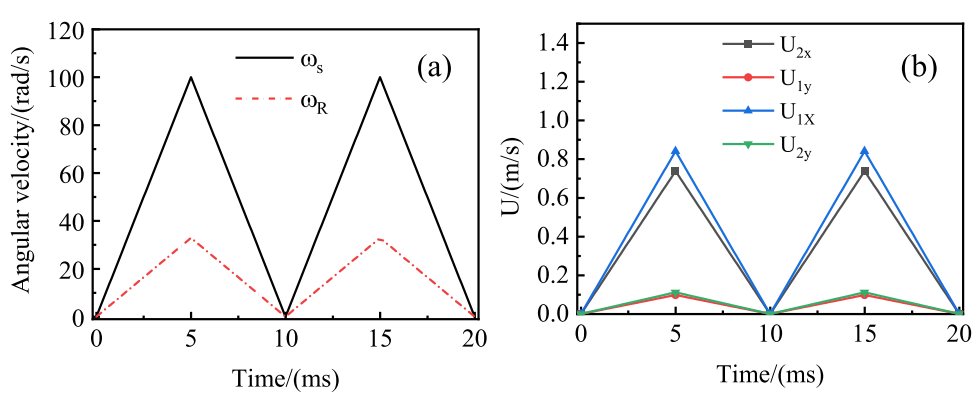

Fig. 14. Angular velocity of roller revolution and screw rotation (a) and entraining velocity (b) during start up and shut down process.

杭州新剑技术转载

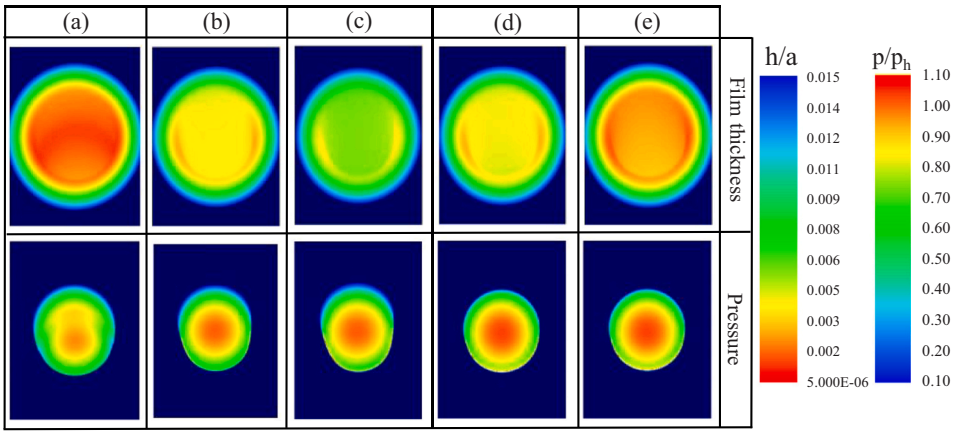

Fig. 15. Film thickness and pressure contours during the start up and shut down process (Smooth). (a) $t = 11$ ms (b) $t = 13$ ms (c) $t = 15$ ms (d) $t = 17$ ms and (e) $t = 20$ ms.

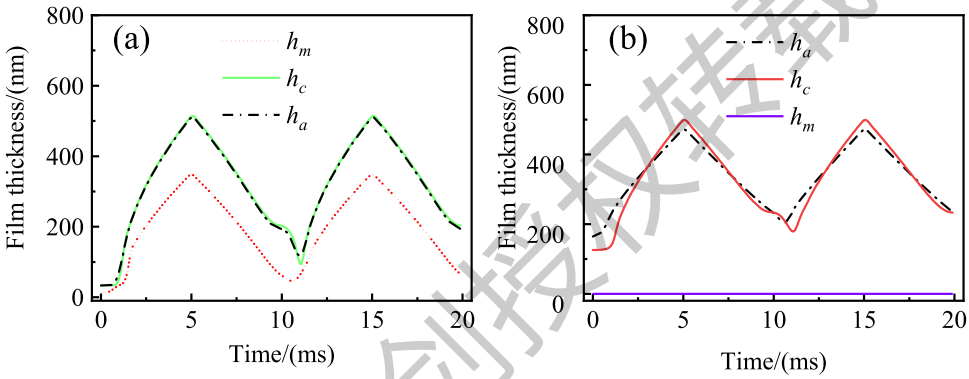

Fig. 16. The variation of film thickness during start up and shut down process. (a) Smooth surface (b) Rough surface.

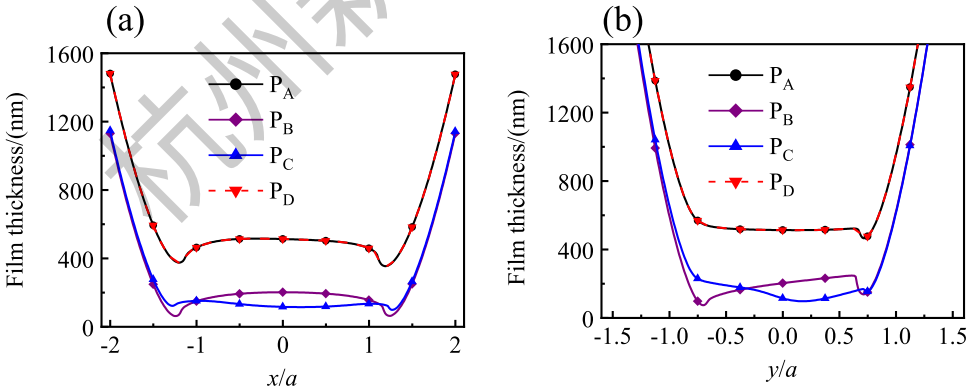

Fig. 17. Film thickness distribution at four selected points (Smooth). (a) Film thickness distribution in the X rolling direction and (b) Film thickness distribution in the Y rolling direction.

5. Conclusion

In this paper, taking the contact geometry, kinematics, load distribution, 3D machined roughness and entrainment angle into consideration, a mixed-EHL model of PRSM was developed. A comprehensive analysis of the effect of different helix angle on lubrication has been explained. The uneven friction between threads and transient behaviors of the start up and shut down process has been executed. The main conclusions of this paper are as follows:

(1) The helix angle that can change the entrainment velocity vector and the equivalent radii of curvature is a key factor of lubrication in the screw-roller interface. And the small helix angle can make the contact interface have an excellent lubrication.

(2) Considering the pitch deviation, the uneven friction distribution that may cause roller axis offset movement is analyzed. Increasing the rotational speed and reducing axial force can decrease the dynamic friction offset moment, thus alleviate the uneven friction distribution and load of the spur ring gear.

杭州新剑技术转载

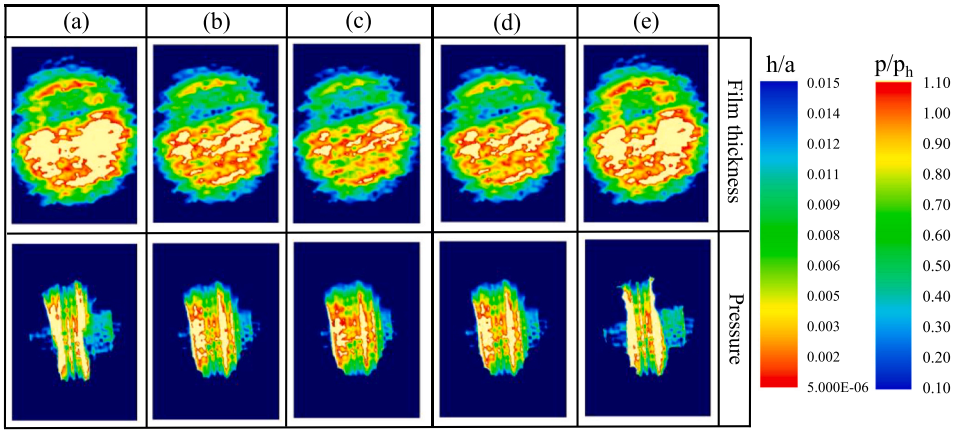

Fig. 18. Film thickness and pressure contours during start up and shut down process (Rough). (a) $t = 11$ ms (b) $t = 13$ ms (c) $t = 15$ ms (d) $t = 17$ ms and (e) $t = 20$ ms.

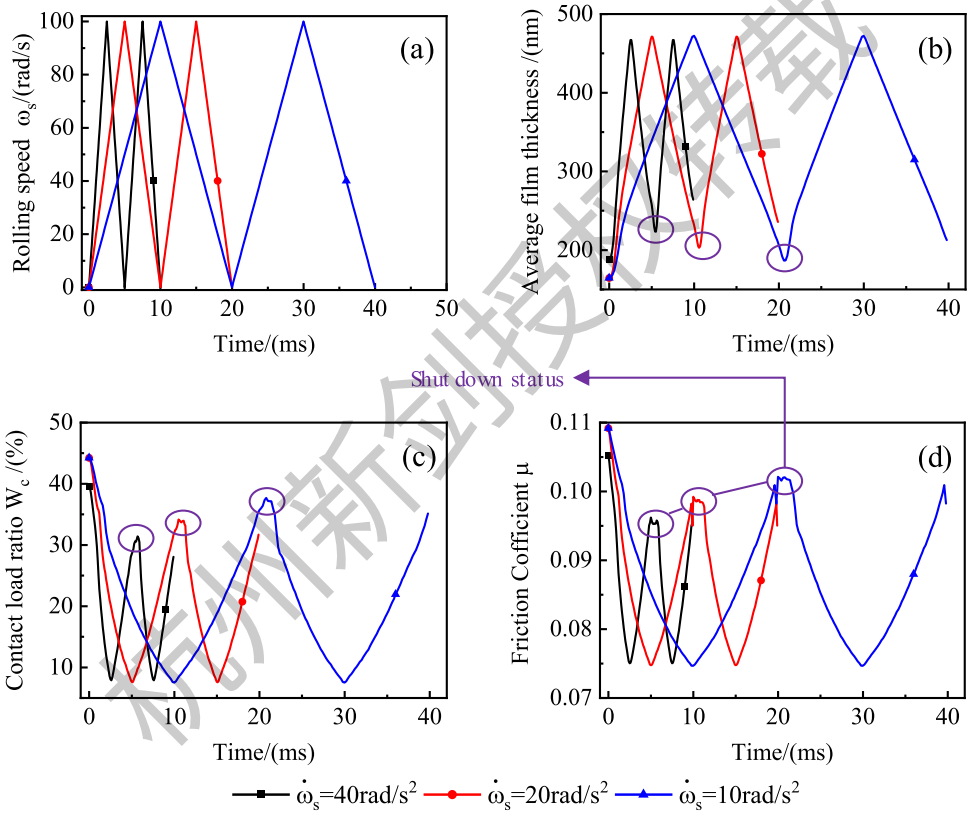

Fig. 19. Effects of angular acceleration on the lubrication during the start up and shut down process.

(3) The lubrication of roller-screw interface during two start up and shut down process is emulated, which shows that larger angular acceleration is beneficial to improve the lubrication at screw-roller interface during the shut down status of back-and-forth motion.

CRediT authorship contribution statement

Guangwu Zhou: Methodology, Conceptualization, Software, Investigation, Writing - original draft. **Yuhao Zhang:** Conceptualization, Writing - original draft, Writing - review & editing, Validation. **Zhongzheng Wang:** Resources, Writing - review & editing. **Wei Pu:** Supervision, Conceptualization, Methodology, Writing - review & editing. All authors have read and agreed to the published version of the manuscript. Authorship must be limited to those who have contributed substantially to the work reported.

Declaration of Competing Interest

The authors declare that they have no known competing financial interests or personal relationships that could have appeared to influence the work reported in this paper.

Acknowledgments

This study was supported by the National Natural Science Foundation of China (Nos. 51875369 and 51605316) and Project Funded by China Postdoctoral Science Foundation (Nos. 2018T110971 and

2017M623027).

References

[1] Aurégan G, Fridrici V, Kapsa P, Rodrigues F. Experimental simulation of rolling–sliding contact for application to planetary roller screw mechanism. Wear 2015;332–333:1176–84.
[2] Ma S, Wu L, Fu X, Li Y, Liu G. Modelling of static contact with friction of threaded surfaces in a planetary roller screw mechanism. Mech Mach Theory 2019;139: 212–36.
[3] Velinsky SA, Chu B, Lasky TA. Kinematics and efficiency analysis of the planetary roller screw mechanism. J Mech Des 2009;131:1–8.
[4] Jones MH, Velinsky SA. Kinematics of roller migration in the planetary roller screw mechanism. J Mech Des 2012;134:1–6.
[5] Jones MH, Velinsky SA. Contact kinematics in the roller screw mechanism. J Mech Des 2013;135:051003.
[6] Jones MH, Velinsky SA, Lasky TA. Dynamics of the planetary roller screw mechanism. J Mech Robot 2016;8:1–6.
[7] Fu XJ, Liu G, Ma SJ, et al. An efficient method for the dynamic analysis of planetary roller screw mechanism. Mech. Mach. Theory 2020;150:103851.
[8] Fu X, Liu G, Tong R, Ma S, Lim TC. A nonlinear six degrees of freedom dynamic model of planetary roller screw mechanism. Mech Mach Theory 2018;119:22–36.
[9] Abevi F, Daidie A, Chaussumier M, Sartor M. Static load distribution and axial stiffness in a planetary roller screw mechanism. J Mech Des 2016;138:012301.
[10] Abevi F, Daidie A, Chaussumier M, Orieux S. Static analysis of an inverted planetary roller screw mechanism. J Mech Robot 2016;8:041020.
[11] Zhang W, Liu G, Ma S, Tong R. Load distribution over threads of planetary roller screw mechanism with pitch deviation. Proc IME C J Mech Eng Sci 2019;233: 4653–66.
[12] Ma S, Liu G, Tong R, Fu X. A frictional heat model of planetary roller screw mechanism considering load distribution. Mech Base Des Struct Mach 2015;43: 164–82.
[13] Xie Z, Xue Q, Wu J, Gu L, Wang L, Song B. Mixed-lubrication analysis of planetary roller screw. Tribology Int 2019;140:105883.
[14] Qiao G, Liu G, Ma S, Wang Y, Li P, Lim TC. Thermal characteristics analysis and experimental study of the planetary roller screw mechanism. Appl Therm Eng 2019;149:1345–58.
[15] Li L, Fu Y, Zheng S, Fu J, Xia T. Friction torque analysis of planetary roller screw mechanism in roller jamming. Math Probl Eng 2020;2020:1–8.
[16] Sandu S, Biboulet N, Nelias D, Abevi F. Analytical prediction of the geometry of contact ellipses and kinematics in a roller screw versus experimental results. Mech Mach Theory 2019;131:115–36.
[17] Venner CH. Multilevel solution of the EHL line and point contact problems. Enschede, Netherlands: University of Twente,; 1991.
[18] Kweh CC, Patching MJ, Evans HP, Snidle RW. Simulation of elastohydrodynamic contacts between rough surfaces. J Tribol 1992;114(3):412–9.
[19] Zhu D, Hu YZ. The study of transition from full film elastohydrodynamic to mixed and boundary lubrication. ASME,; 1999. p. 150–6.
[20] Zhu D, Ai X. Point contact EHL based on optically measured three-dimensional rough surfaces. ASME J Tribol, 119; 1997. p. 375–84.
[21] Zhu D. On some aspects in numerical solution of thin-film and mixed EHL. Proc Inst Mech Eng Part J 2007;221:561–79.
[22] Hu YZ, Zhu D. A full numerical solution to the mixed lubrication in point contacts. ASME J Tribol, 122; 2000. p. 1–9.
[23] Wang WZ, Wang H, Liu YC, Hu YZ, Zhu D. A comparative study of the methods for calculation of surface elastic deformation. Proc Inst Mech Eng Part J 2003;217: 145–53.
[24] Liu Y, Wang QJ, Wang W, et al. Effects of differential scheme and mesh density on EHL film thickness in point contacts. ASME J Tribol, 128; 2006. p. 641–53.
[25] He T, Zhu D, Wang J, et al. Experimental and numerical investigations of thestribeck curves for lubricated counterformal contacts. ASME J Tribol, 139; 2017, 021505.
[26] Lubrecht AA, Biboulet N, Venner CH. Boundary layers: unifying the impact and rolling EHL point contacts. Tribol Int 2018;126:186–91.
[27] Houpert LG, Hamrock BJ. Fast approach for calculating film thicknesses and pressur-es in elastohydrodynamically lubricated contacts at heavy loads. ASME J Tribol, 108; 1986. p. 411–20.
[28] Hou KP, Zhu D, Wen SZ. An inverse solution to the point contact EHL problem under heavy loads. ASME J Tribol, 109; 1987. p. 432–6.
[29] Ai X. Numerical analyses of elastohydrodynamically lubricated line and point contacts with rough surfaces by using semi-system and multigrid methods. Evanston, USA: Northwestern University,; 1993.
[30] Lubrecht AA, Ten Napel WE, Bosma R. Multigrid, an alternative method for calculating film thickness and pressure profiles in elastohydrodynamically lubricated line contacts. J Tribol 1987;108:437–43.
[31] Lubrecht AA. The numerical solution of elastohydrodynamic lubricated line and point contact problems using multi-grid techniques. Netherlands: University of Twente,; 1987.
[32] Wang J, Qu S, Yang P. Simplified multigrid technique for the numerical solution to the steady-state and transient EHL line contacts and the arbitrary entrainment EHL point contacts. Tribol Int 2001;34(3):191–202.
[33] Pu W, Wang J, Zhang Y, Zhu D. A theoretical analysis of the mixed elastohydrodynamic lubrication in elliptical contacts with an arbitrary entrainment angle. J Tribol 2014;136:041505.
[34] Wang Z, Pu W, He T, Wang J, Cao W. Numerical simulation of transient mixed elastohydrodynamic lubrication for spiral bevel gears. Tribol Int 2019;139:67–77.
[35] Zhu D, Wang J, Wang QJ. On the stribeck curves for lubricated counterformal contacts of rough surfaces. J Tribol 2015;137(2):021501.
[36] Zhu D, Wang QJ. Elastohydrodynamic lubrication: a gateway to interfacial mechanics—review and prospect. ASME J Tribol 2011;133(4):1–14.
[37] Du X, Chen Bk, Zheng ZD. Investigation on mechanical behavior of planetary roller screw mechanism with the effects of external loads and machining errors. Tribology Int 2021;154:106689.
[38] Habchi W, Eyheramendy D, Bair S, Vergne P, Morales-Espejel G. Thermal elastohydrodynamic lubrication of point contacts using a Newtonian/generalized Newtonian lubricant. Tribol Lett 2008;30(1):41–52.
[39] Hamrock BJ, Dowson D. Isothermal elastohydrodynamic lubrication of point contacts: part I-theoretical formulation. ASME J Lubr Technol 1976;98:223–9.
[40] Liu S, Wang QJ, Liu G. A versatile method of discrete convolution and FFT (DC-FFT) for contact analyses. Wear 2000;243(1–2):101–11.
[41] Zhu D, Wang QJ. On the λ ratio range of mixed lubrication. Proc Inst Mech Eng Part J 2012;226(12):1010–22.

杭州新剑摘录